

Efficient and accurate linear algebraic methods for large-scale electronic structure calculations with nonorthogonal atomic orbitals

H. Teng,^{1,*} T. Fujiwara,^{1,2,†} T. Hoshi,^{2,3} T. Sogabe,^{2,4} S.-L. Zhang,^{2,5} and S. Yamamoto^{2,6}

¹Center for Research and Development of Higher Education, The University of Tokyo, Bunkyo-ku, Tokyo, 113-8656, Japan

²Core Research for Evolutional Science and Technology, Japan Science and Technology Agency (CREST-JST), Japan

³Department of Applied Mathematics and Physics, Tottori University, Tottori 680-8550, Japan

⁴School of Information Science and Technology, Aichi Prefecture University, Nagakute-cho, Aichi 480-1198, Japan

⁵Department of Computational Science and Engineering, Nagoya University, Chikusa-ku, Nagoya 464-8603, Japan

⁶School of Computer Science, Tokyo University of Technology, Katakura-machi, Hachioji, Tokyo 192-0982, Japan

(Received 13 August 2010; revised manuscript received 1 December 2010; published 6 April 2011)

The need for large-scale electronic structure calculations arises recently in the field of material physics, and efficient and accurate algebraic methods for large simultaneous linear equations become greatly important. We investigate the generalized shifted conjugate orthogonal conjugate gradient method, the generalized Lanczos method, and the generalized Arnoldi method. They are the solver methods of large simultaneous linear equations of the one-electron Schrödinger equation and map the whole Hilbert space to a small subspace called the Krylov subspace. These methods are applied to systems of fcc Au with the NRL tight-binding Hamiltonian [F. Kirchoff *et al.*, *Phys. Rev. B* **63**, 195101 (2001)]. We compare results by these methods and the exact calculation and show them to be equally accurate. The system size dependence of the CPU time is also discussed. The generalized Lanczos method and the generalized Arnoldi method are the most suitable for the large-scale molecular dynamics simulations from the viewpoint of CPU time and memory size.

DOI: [10.1103/PhysRevB.83.165103](https://doi.org/10.1103/PhysRevB.83.165103)

PACS number(s): 71.15.Pd, 02.70.Ns, 02.60.Dc

I. INTRODUCTION

In recent years, molecular dynamics (MD) simulations with electronic structure calculations in nanoscale structures have attracted much attention. One needs a large size of systems of several hundred thousands atoms with a few hundred picoseconds (or more longer time) process in order to investigate characteristics of nanoscale systems such as phenomena of competition between different physical principles or phenomena of the multiphysics, e.g., energy competition between the strain field and chemical bonds.¹⁻⁴ Several requirements for large-scale MD simulation with electronic structure calculations are contradictory to each other, e.g., total energy accuracy versus larger system size or longer physical time of processes.

There are several approaches for large-scale MD simulations:⁵ (a) the Fermi operator expansion,⁶ (b) the divide-and-conquer method,⁷ and (c) the minimization method (the density matrix minimization⁸ or the wave-function minimization⁹). Another classification may be the one accorded as the basis set of wave functions: (a) the plane-wave basis set and switching between the real-space and k -space representation,¹⁰ and (b) localized orbitals¹¹ or tight-binding basis set.¹² Computation with a “massively parallel machine” is also an important issue.

An important aspect is the development of novel algebraic algorithm for extra-large-scale systems. The most general and important algorithm may be the linear algebra solving the simultaneous linear equations

$$(z - H)\mathbf{x} = \mathbf{b}, \quad (1)$$

where H is the self-adjoint or real symmetric matrix, \mathbf{b} is a given vector, $z = \varepsilon + i\eta$, ε is an energy parameter, and η is an infinitesimally small positive number, respectively. Solutions

of Eq. (1) relate to the standard eigenvalue problem $(\varepsilon - H)\mathbf{x} = 0$. We developed the subspace diagonalization method and the shifted conjugate orthogonal conjugate gradient (COCG) method.¹³⁻¹⁶ Then, the methods were applied to the fracture propagation and surface formation in Si crystals with the tight-binding Hamiltonian based on an orthogonal basis set.^{1,2} On the other hand, since its Hamiltonian is described by the tight-binding Hamiltonian based on a nonorthogonal basis set, the problem of the formation of Au multishell helical nanowires was solved by the exact diagonalization method.^{3,4}

Development of efficient linear algebraic methods has been, so far, mainly based on the orthogonal basis sets.^{13,14,17-19} However, localized basis wave functions are generally nonorthogonal and it is much more desirable to generalize the methods to the case of a nonorthogonal basis set. The most popular strategy of the generalized eigenvalue problem (represented by the nonorthogonal basis set) would be the transformation to the standard eigenvalue problem.¹⁹ Our target in this paper is to solve simultaneous linear equations with self-adjoint or real symmetric matrix S :

$$(zS - H)\mathbf{x} = \mathbf{b}, \quad (2)$$

which relates to the generalized eigenvalue problem $(\varepsilon S - H)\mathbf{x} = 0$. We will investigate efficient methods of solving Eq. (2) with a complex energy variable z when the matrix size of H and S is huge. Several algebraic algorithms will be discussed and directly applied to a tight-binding Hamiltonian based on nonorthogonal atomic orbitals in large-scale systems.

The structure of this paper is as follows. In Sec. II, the idea of nonorthogonal atomic orbitals and physical properties (e.g., the band energy, the local and partial density of states, numbers of occupied electron states, the chemical potential, etc.) are summarized. Sections III, IV, and V explain three different algorithms of large-scale linear equations, i.e., the

generalized shifted conjugate orthogonal conjugate gradient method (GsCOCG), the generalized Lanczos method, and the generalized Arnoldi method, which generate the Krylov subspace from the whole Hilbert space. In these sections, numerical examples are presented by using the NRL tight-binding Hamiltonian. The generalized Lanczos method becomes applicable to actual large systems with a high accuracy if one uses the modified Gram-Schmidt reorthogonalization to maintain the orthogonality of generated basis vectors. In Sec. VI, we compare the CPU times of each algorithm and discuss the applicability to large-scale electronic structure calculations and MD simulations. Section VII presents our conclusions. The examples without reorthogonalization in the generalized Lanczos method are shown and discussed in Appendix A. Appendix B is devoted to discussing the consistency between the total energy and force.

II. THEORETICAL BACKGROUND

A. Nonorthogonal basis set and S orthogonalization

We define two sets of wave functions $\{\phi_i(\mathbf{r})\}$ and $\{\psi_\alpha(\mathbf{r})\}$, where $\{\phi_i(\mathbf{r})\}$ is the nonorthogonal (normalized) basis set (e.g., atomic orbitals and i denote an atomic site and energy level), and $\{\psi_\alpha(\mathbf{r})\}$ is the orthonormalized basis set. Then, the overlap matrix S_{ij} and the Hamiltonian matrix H_{ij} are defined as

$$S_{ij} = \langle \phi_i | \phi_j \rangle = \int \phi_i^* \phi_j d\mathbf{r}, \quad S_{ii} = 1, \quad (3)$$

$$H_{ij} = \langle \phi_i | \hat{H} | \phi_j \rangle = \int \phi_i^* \hat{H} \phi_j d\mathbf{r}, \quad (4)$$

where \hat{H} is the Hamiltonian operator. The orthonormal basis set $\{\psi_\alpha(\mathbf{r})\}$ can be expanded in terms of $\{\phi_j\}$ as

$$\psi_\alpha(\mathbf{r}) = \sum_i \phi_i(\mathbf{r}) w_i^{(\alpha)} \quad (5)$$

and the orthogonality relation is expressed as

$$\langle \psi_\alpha | \psi_\beta \rangle = \sum_{ij} w_i^{(\alpha)*} w_j^{(\beta)} S_{ij} \quad (6)$$

$$\equiv (\mathbf{w}^{(\alpha)}, \mathbf{w}^{(\beta)})_S = \delta_{\alpha\beta}, \quad (7)$$

where $\mathbf{w}^{(\alpha)} = (w_1^{(\alpha)}, w_2^{(\alpha)}, \dots)^t$. We call the representation $(\mathbf{w}^{(\alpha)}, \mathbf{w}^{(\beta)})_S$ the S product and the relation (7) is the S orthogonalization of basis vectors $\mathbf{w}^{(\alpha)}$.

When $\psi_\alpha(\mathbf{r})$ satisfies the Schrödinger equation

$$\hat{H} \psi_\alpha(\mathbf{r}) = \varepsilon_\alpha \psi_\alpha(\mathbf{r}), \quad (8)$$

the coefficients $\{w_i^{(\alpha)}\}$ should be elements of an eigenvector of a simultaneous linear equation in the ϕ representation

$$\sum_i H_{ji} w_i^{(\alpha)} = \varepsilon_\alpha \sum_i S_{ji} w_i^{(\alpha)} \quad (9)$$

or, in matrix-vector form,

$$H \mathbf{w}^{(\alpha)} = \varepsilon_\alpha S \mathbf{w}^{(\alpha)}. \quad (10)$$

Matrices $H = (H_{ij})$ and $S = (S_{ij})$ are self-adjoint in the ϕ representation.

B. Green's function and local and partial density of states represented by the nonorthogonal basis set

The Green's function operator \hat{G} is defined as

$$\hat{G}(z) = \{(\varepsilon + i\eta)\hat{1} - \hat{H}\}^{-1}, \quad (11)$$

where $\hat{1}$ is the identity operator and $z = \varepsilon + i\eta$. Elements of the Green's function matrix can then be written as

$$G_{ij}(z) = \langle \phi_i | \hat{G}(z) | \phi_j \rangle = \{S(zS - H)^{-1} S\}_{ij} \quad (12)$$

$$= \sum_{k,l} S_{ik} \left\{ \sum_{\alpha} w_k^{\alpha*} \frac{1}{z - \varepsilon_{\alpha}} w_l^{\alpha} \right\} S_{lj}. \quad (13)$$

The local (partial) densities of states (DOS) are expressed in the ϕ representation as follows:

$$D_{ij}(\varepsilon) = -\frac{1}{\pi} \text{Im}[G(z)S^{-1}]_{ij}. \quad (14)$$

The normalization of the Green's functions and the local and partial density of states is then

$$\left(-\frac{1}{\pi}\right) \int_{-\infty}^{\infty} d\varepsilon \text{Im} G_{ij}(z) = \langle \phi_i | \phi_j \rangle = S_{ij}, \quad (15)$$

$$\int_{-\infty}^{\infty} d\varepsilon D_{ii}(\varepsilon) = 1. \quad (16)$$

C. Total band energy and Green's function

1. Density matrix and energy density matrix

In the simulation process, the density matrix ρ_{ij} and the energy density matrix π_{ij} appear repeatedly in the calculation of the Mulliken charge, the total energy, and forces,²⁰ the definition of which may be

$$\rho_{ij} = \left(-\frac{1}{\pi}\right) \text{Im} \int d\varepsilon \sum_{\alpha} f(\varepsilon_{\alpha}) \frac{w_i^{(\alpha)*} w_j^{(\alpha)}}{z - \varepsilon_{\alpha}} \quad (17)$$

$$= \sum_{\alpha} f(\varepsilon_{\alpha}) w_i^{(\alpha)*} w_j^{(\alpha)}, \quad (18)$$

$$\pi_{ij} = \left(-\frac{1}{\pi}\right) \text{Im} \int d\varepsilon \varepsilon \sum_{\alpha} f(\varepsilon_{\alpha}) \frac{w_i^{(\alpha)*} w_j^{(\alpha)}}{z - \varepsilon_{\alpha}} \quad (19)$$

$$= \sum_{\alpha} f(\varepsilon_{\alpha}) \varepsilon_{\alpha} w_i^{(\alpha)*} w_j^{(\alpha)}, \quad (20)$$

where $f(\varepsilon)$ is the Fermi-Dirac function $f(\varepsilon) = \{1 + \exp[(\varepsilon - \mu)/\tau]\}^{-1}$, where μ and τ are the chemical potential and temperature.

2. Physical property

The chemical potential μ should be determined by the equation for the total electron number N_{tot} :

$$N_{\text{tot}} = 2 \sum_i \int d\varepsilon f(\varepsilon) D_{ii}(\varepsilon) \quad (21)$$

$$= \sum_{ij\alpha} S_{ij} \left(-\frac{2}{\pi}\right) \text{Im} \int d\varepsilon f(\varepsilon_{\alpha}) \frac{w_j^{(\alpha)*} w_i^{(\alpha)}}{z - \varepsilon_{\alpha}} \quad (22)$$

$$= 2 \sum_{ij} S_{ij} \rho_{ji}, \quad (23)$$

where a factor “2” is the spin degeneracy.

The total band energy of the system is given as

$$E_{\text{tot}} = 2 \sum_{\alpha}^{\text{occ}} \varepsilon_{\alpha} = 2 \sum_{\alpha} \varepsilon_{\alpha} f(\varepsilon_{\alpha}) \quad (24)$$

$$= -\frac{2}{\pi} \text{Im} \sum_i \int d\varepsilon \varepsilon f(\varepsilon) [G(z)S^{-1}]_{ii}, \quad (25)$$

where the summation $\sum_{\alpha}^{\text{occ}}$ runs over the occupied states. This equation can be expressed by the density of states, the density matrix, or the energy density matrix as

$$E_{\text{tot}} = 2 \sum_i \int d\varepsilon \varepsilon f(\varepsilon) D_{ii}(\varepsilon) \quad (26)$$

$$= 2 \sum_{ij} \rho_{ij} H_{ji} \quad (27)$$

$$= 2 \sum_{ij} S_{ij} \pi_{ji}. \quad (28)$$

Moreover, any physical property can be expressed by using the density matrix as

$$\begin{aligned} \langle X \rangle &= \left(-\frac{2}{\pi} \right) \int d\varepsilon f(\varepsilon) \sum_{ij} X_{ij} \text{Im}[S^{-1}G(z)S^{-1}]_{ji} \\ &= 2 \sum_{ij} X_{ij} \rho_{ji}. \end{aligned} \quad (29)$$

The expressions (27) and (28) and also (29) are satisfied not only in the whole Hilbert space but also in the mapped subspace in which we construct approximate eigenstates.

Now we have obtained three different expressions [Eqs. (21)–(23)] for N_{tot} and [Eqs. (26)–(28)] for E_{tot} . These expressions normally give different values because we usually use finite values of the energy interval η and approximate eigenstates in the mapped subspace. Fortunately, if the formula $\sum_{ij} \rho_{ij} H_{ji} = \sum_{ij} S_{ij} \pi_{ji}$ is satisfied, the consistency between the total band energy and the force can be kept as shown in Appendix B.

III. GENERALIZED SHIFTED COCG METHOD

We developed the shifted COCG method for large-scale linear equation (1).^{14,15,21} It was shown that the convergence behavior can be monitored by observing the behavior of the “residual norm.” The shifted COCG method is generalized for Eq. (2) in this section.

A. Definition of the problem

The eigenvalue problem of the stationary Schrödinger equation is equivalent to the scattering problem

$$(z\hat{1} - \hat{H})\psi(\mathbf{r}) = \chi(\mathbf{r}), \quad (30)$$

where $z = \varepsilon + i\eta$ and ε is an energy parameter of incident waves. The wave function $\psi(\mathbf{r})$ is expanded by the set of nonorthogonal atomic orbitals $\{\phi_j\}$:

$$\psi(\mathbf{r}) = \sum_j \phi_j(\mathbf{r}) x_j(z). \quad (31)$$

Substituting Eq. (31) into (30), one obtains the generalized linear equations

$$(zS - H)\mathbf{x}(z) = \mathbf{b}, \quad (32)$$

where the j th component of the vector \mathbf{b} is $b_j = \langle \phi_j | \chi \rangle$. The solution of the linear equation $\mathbf{x}(z)$ is then

$$\mathbf{x}(z) = (zS - H)^{-1} \mathbf{b} = S^{-1}G(z)S^{-1} \mathbf{b} \quad (33)$$

with the help of Eq. (12). By setting a vector \mathbf{b} as

$$\mathbf{b} = \mathbf{e}_j = (0, 0, \dots, 0, \underbrace{1}_j, 0, 0, \dots)^t, \quad (34)$$

we can get the corresponding solution $\mathbf{x}^j(z)$ as

$$\mathbf{x}^j(z) = S^{-1}G(z)S^{-1} \mathbf{e}_j. \quad (35)$$

The product of \mathbf{e}_i and \mathbf{x}^j (not the S product), the i th element of a vector \mathbf{x}^j , is identical just to the energy component of the density matrix $\rho_{ij}(\varepsilon)$:

$$\rho_{ij}(\varepsilon) = -\frac{1}{\pi} \text{Im}[\mathbf{e}_i^t \cdot \mathbf{x}^j(\varepsilon + i\eta)], \quad (36)$$

which relates to the local DOS as

$$D_{ii}(\varepsilon) = \sum_k S_{ik} \rho_{ki}(\varepsilon). \quad (37)$$

Then, the density matrix and the energy density matrix are given by the integrations of $\rho_{ij}(\varepsilon)$ as

$$\rho_{ij} = \int d\varepsilon f(\varepsilon) \rho_{ij}(\varepsilon), \quad (38)$$

$$\pi_{ij} = \int d\varepsilon \varepsilon f(\varepsilon) \rho_{ij}(\varepsilon). \quad (39)$$

It should be noted here that there are no quantities of eigenenergies in the Krylov subspace and we should use the calculation procedure through $\rho_{ij}(\varepsilon)$ rather than the calculation of Eqs. (18) and (20). Their resultant values depend on the interval of energy mesh points for the energy integration and a fictitious finite value of η .

B. Generalized shifted conjugate orthogonal conjugate gradient (GsCOCG) method

For the nonorthogonal basis set, we can generalize the shifted COCG procedure, named the generalized shifted COCG (GsCOCG) method.²² The linear equations of the seed energy σ_s and the shift energy σ , respectively, are written as

$$(S^{-1}A + \sigma_s 1)\mathbf{x} = S^{-1}\mathbf{b}, \quad (40)$$

$$(S^{-1}A + \sigma 1)\mathbf{x}^{(i)} = S^{-1}\mathbf{b}, \quad (41)$$

where the matrix A is defined as

$$A = z_{\text{ref}}S - H \quad (42)$$

with an arbitrary reference energy $z_{\text{ref}} = \varepsilon_{\text{ref}} + i\eta$, 1 is the unit matrix, and $\mathbf{b} = \mathbf{e}_j$. The seed energy and the shift energy are given as $\varepsilon_s = \varepsilon_{\text{ref}} + \sigma_s$ and $\varepsilon = \varepsilon_{\text{ref}} + \sigma$.

Following the procedure of the shifted COCG method,^{15,16} we try to find iterative n th solutions \mathbf{x}_n in the Krylov subspace defined as

$$\begin{aligned} K_n(S^{-1}A + \sigma_s I, S^{-1}\mathbf{b}) \\ = \text{Span}\{S^{-1}\mathbf{b}, S^{-1}AS^{-1}\mathbf{b}, (S^{-1}A)^2S^{-1}\mathbf{b}, \\ \dots, (S^{-1}A)^n S^{-1}\mathbf{b}\}. \end{aligned} \quad (43)$$

This yields the residual vector $\mathbf{r}'_n = S^{-1}\mathbf{b} - (S^{-1}A + \sigma_s I)\mathbf{x}_n$ to be²²

$$\mathbf{r}'_n \perp K_n[(S^{-1}A + \sigma_s I)^\dagger, \mathbf{b}^*], \quad (44)$$

where B^\dagger is the Hermitian conjugate matrix of B and \mathbf{b}^* is the complex conjugate vector of \mathbf{b} . The actual algorithms may be as follows. Under the initial conditions

$$\mathbf{x}_0 = \mathbf{p}_{-1} = \mathbf{0}, \quad (45)$$

$$\mathbf{r}_0 = \mathbf{b}, \quad (46)$$

$$\alpha_{-1} = 1, \quad \beta_{-1} = 0, \quad (47)$$

and a definition $\mathbf{r}'_0 = S^{-1}\mathbf{r}_0$, we evaluate the following equations for the seed energy σ_s iteratively for $n = 0, 1, 2, \dots$:

$$\begin{aligned} \mathbf{p}_n &= \mathbf{r}'_n + \beta_{n-1}\mathbf{p}_{n-1}, \\ \alpha_n &= \frac{(\mathbf{r}'_n, \mathbf{r}'_n)_S}{[\mathbf{p}_n, S^{-1}(A + \sigma_s S)\mathbf{p}_n]_S}, \\ \mathbf{x}_{n+1} &= \mathbf{x}_n + \alpha_n \mathbf{p}_n, \\ \mathbf{r}_{n+1} &= \mathbf{r}_n - \alpha_n(A + \sigma_s S)\mathbf{p}_n, \\ \mathbf{r}'_{n+1} &= S^{-1}\mathbf{r}_{n+1}, \\ \beta_n &= \frac{(\mathbf{r}'_{n+1}, \mathbf{r}'_{n+1})_S}{(\mathbf{r}'_n, \mathbf{r}'_n)_S}. \end{aligned} \quad (48)$$

The important point here is our use of $\mathbf{r}'_n = S^{-1}\mathbf{r}_n$. In actual procedure, we employ a form $\mathbf{r}_n = S\mathbf{r}'_n$ at each iteration step by the CG method. Since the overlap matrix S is real symmetric, positive definite, and sparse, the convergence of CG iteration can be fast.

The basic theorem of the Krylov subspace is the invariance of the subspace under an energy shift σ . The other very basic theorem is the *collinear residual*²³

$$\mathbf{r}_n^\sigma = \frac{1}{\pi_n^\sigma} \mathbf{r}_n. \quad (49)$$

Owing to these theorems, once we solve the set of equations for the seed energy σ_s , we can obtain the results for any shift energy σ only by scalar multiplications. The recurrence equations for shift energies are given (all the quantities are denoted by the superscript σ), with initial values $\pi_{-1}^\sigma = \pi_0^\sigma = 1$, as follows:

$$\pi_{n+1}^\sigma = \{1 + \alpha_n(\sigma - \sigma_s)\}\pi_n^\sigma + \frac{\beta_{n-1}}{\alpha_{n-1}}\alpha_n(\pi_n^\sigma - \pi_{n-1}^\sigma) \quad (50)$$

and

$$\mathbf{x}_{n+1}^\sigma = \mathbf{x}_n^\sigma + \alpha_n^\sigma \mathbf{p}_n^\sigma \quad (51)$$

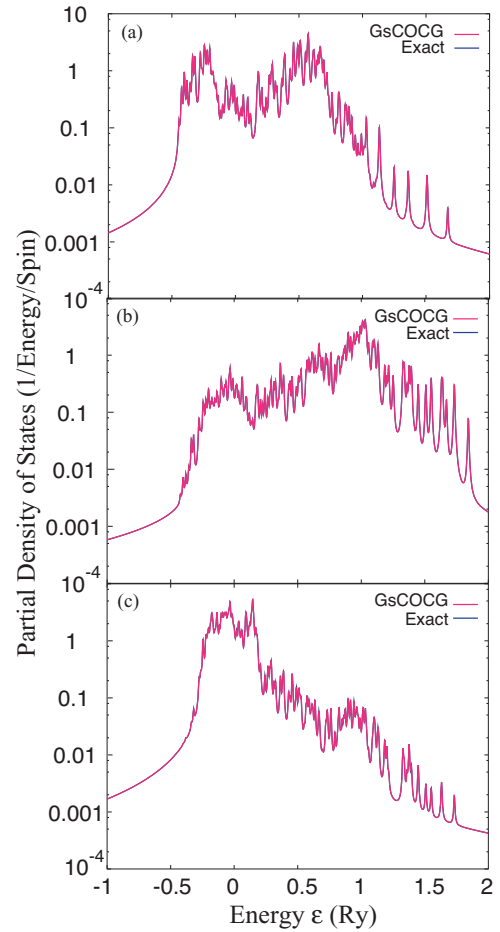


FIG. 1. (Color online) Partial density of states for a system of Au 864 atoms by the NRL tight-binding Hamiltonian (Ref. 24) normalized to unity. (a) s orbitals, (b) p orbitals, and (c) d orbitals. Comparison is for the GsCOCG and the exact calculation, which are almost identical to each other. Parameters in GsCOCG calculations are $\eta = 10^{-3}$ Ry, $\tau = 5\eta$. The energy interval of mesh points is 10^{-4} Ry. See Figs. 4, 5, and 7 for comparison.

with

$$\begin{aligned} \alpha_n^\sigma &= \frac{\pi_n^\sigma}{\pi_{n+1}^\sigma} \alpha_n, \\ \beta_{n-1}^\sigma &= \left(\frac{\pi_{n-1}^\sigma}{\pi_n^\sigma}\right)^2 \beta_{n-1}, \\ \mathbf{p}_n^\sigma &= \frac{1}{\pi_n^\sigma} \mathbf{r}'_n + \beta_{n-1}^\sigma \mathbf{p}_{n-1}^\sigma. \end{aligned}$$

Partial densities of states are shown in Fig. 1 for a system of Au 864 atoms by the NRL tight-binding Hamiltonian,²⁴ in comparison with those by the exact calculation. In order to see the behavior of the peak positions and the tail of the peaks, the figures are drawn in the logarithmic scale. Two lines of the GsCOCG and the exact calculation overlap each other almost completely, and one can recognize an excellent agreement between the two different calculations.

C. Residual norm and convergence behavior

The useful characteristic property of the GsCOCG method is the capability of monitoring the norm of residual vectors.¹⁴ The residual vectors for the seed and shift equations with an energy ε_k (with $\mathbf{b} = \mathbf{e}_j$ and $\sigma_k = \varepsilon_k - \varepsilon_{\text{ref}}$) are $\mathbf{r}_n^{(s,j)}$ and $\mathbf{r}_n^{(k,j)}$, respectively, and the mapped residual vectors for the seed and shift equations $\mathbf{r}_n'^{(s,j)} = S^{-1}\mathbf{r}_n^{(s,j)}$ and $\mathbf{r}_n'^{(k,j)} = S^{-1}\mathbf{r}_n^{(k,j)}$. We usually need only elements of the density matrix among near-sited orbital pairs connected by nonzero elements of the Hamiltonian or overlap matrices, and the convergence monitoring is necessary for these components.¹⁴ Therefore, in order to monitor the convergence behavior, we adopt the “residual norm” defined as

$$\|\mathbf{r}_n'^{(s/k,j)}\|^2 \equiv \sum_i^{H_{ij} \neq 0} |\mathbf{e}_i^t \cdot \mathbf{r}_n'^{(s/k,j)}|^2. \quad (52)$$

Furthermore, since the residual norm is different among different energy points, the average quantity (“average residual norm”) should be defined as¹⁴

$$\begin{aligned} R_n^{(j)} &\equiv \frac{1}{N_{\text{ene}}} \sum_k^{N_{\text{ene}}} \|\mathbf{r}_n'^{(k,j)}\|^2 \\ &= \|\mathbf{r}_n'^{(s,j)}\|^2 \frac{1}{N_{\text{ene}}} \sum_k^{N_{\text{ene}}} \frac{1}{|\pi_k|^2}, \end{aligned} \quad (53)$$

where N_{ene} is the number of energy points.

The convergence behavior of the residual norm for different seed energies is shown in Fig. 2(a). The convergence at the energy of the low DOS is very fast because the eigenstate can be constructed by a small number of basis states. The convergence of the averaged norm is shown in Fig. 2(b), which confirms numerically the fact that the average residual norm (and all the physical quantities) does not depend sensitively on the choice of a seed energy.

D. Seed-switching technique

When one chooses a seed energy in an energy range of rapid convergence, the spectra at majority energy points have not been converged yet and one should restart the calculation with a new seed energy as seen in Fig. 2(a). The most desirable seed energy may be one of the largest (partial) DOS because the convergence at these points is the slowest.

However, even if one chooses a starting seed energy in the highest DOS region and the residual norm at the seed energy reaches the convergence criterion, it often happens that there still remain several energy points (regions) where the residual norm has not been small enough. Fortunately, the shifting energy does not need any additional heavy computational task but rather several scalar manipulations such as Eq. (50). Because of this property of shifting energy, a choice of a seed energy σ_s can be arbitrary. As shown in Fig. 2(b), even if we start with an improper seed energy and switch a seed, the total iteration times for desired convergence over the whole energy range are not very different. The *seed switching* is a very efficient technique to avoid restarting the calculation from the beginning with a new seed energy.^{16,25} One chooses a new seed energy σ_s^{new} and can continue the calculation without

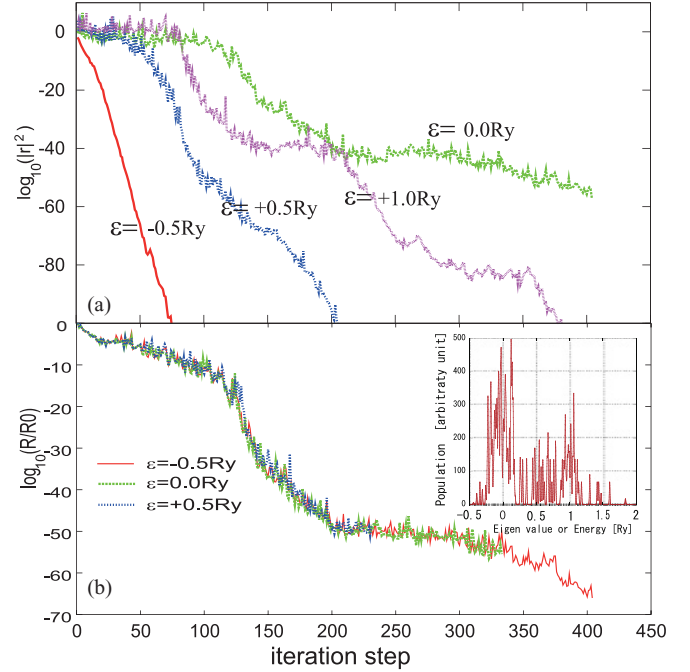


FIG. 2. (Color online) Convergence behavior of residual norms for a system of Au 256 atoms by the NRL tight-binding Hamiltonian (Ref. 24). The spectrum extends between -0.5 and 1.5 Ry. The inset in (b) shows the total density of states $D(\varepsilon) = \sum_i D_{ii}(\varepsilon)$, where we use a finite imaginary number in the energy and the profile is of dense spiky peaks. (a) Residual norm $\|\mathbf{r}_n^{(s,j)}\|$ at several energy points $\varepsilon = -0.5, 0.0, 0.5,$ and 1.0 Ry for the s orbital. (b) Average residual norms $R_n^{(j)}$ with different three seed energies ($-0.5, 0.0,$ and 0.5 Ry) for the s orbital and they all overlap with each other.

discarding the information of the previous calculation with the old σ_s by using the shift property. Figure 3 shows the behavior of the residual norms in the seed-switching process.

IV. GENERALIZED LANCZOS PROCESS AND DENSITY OF STATES

The three-term recursive relation used in the GsCOCG method leads us to the generalization of the Lanczos method.^{18,19,26} As far as we know, the generalization of the Lanczos method was presented first in Ref. 18. In this section, we will stress that the generalized Gram-Schmidt reorthogonalization process makes the generalized Lanczos method practically useful and also the use of Eqs. (18) and (20) gives very efficient and accurate results.

A. Generalized Lanczos process

First we define a matrix \mathcal{H} as

$$\mathcal{H} \equiv S^{-1}H, \quad (54)$$

which is not self-adjoint but still satisfies the *quasi-Hermitian* property in the S product

$$(\mathbf{v}, \mathcal{H}\mathbf{u})_S = (\mathcal{H}\mathbf{v}, \mathbf{u})_S. \quad (55)$$

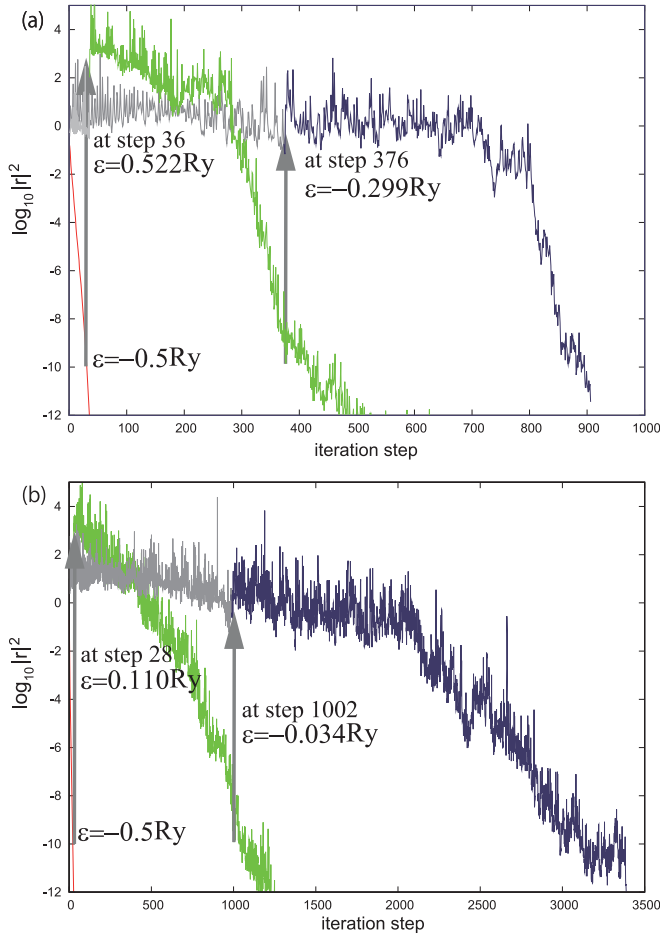


FIG. 3. (Color online) Residual norm at the seed energies for a system of Au 864 atoms by the NRL tight-binding Hamiltonian (Ref. 24) in (a) s orbitals and (b) d orbitals. (a) Seed switches to 0.522 Ry from -0.5 Ry at the 36th step and to -0.299 Ry at the 376th step in the s -orbital case. (b) Seed switches to 0.110 Ry from -0.5 Ry at the 28th step and to -0.034 Ry at the 1002nd step in the d -orbital case. Once the calculation using one seed is converged and full convergence has not been achieved, one should choose the next seed and continue the calculation. The gray lines show the residual norm by energy shift r_n^σ before seed switching.

We can construct the three-term procedure of the Lanczos process ($n = 0, 1, \dots$) as^{18,19}

$$\mathcal{H}\mathbf{u}^n = a_n\mathbf{u}^n + b_{n+1}\mathbf{u}^{n+1} + b_n\mathbf{u}^{n-1}, \quad (56)$$

where

$$\begin{aligned} a_n &= (\mathbf{u}^n, \mathcal{H}\mathbf{u}^n)_S, \\ b_{n+1}^2 &= \{(\mathcal{H} - a_n)\mathbf{u}^n - b_n\mathbf{u}^{n-1}, (\mathcal{H} - a_n)\mathbf{u}^n - b_n\mathbf{u}^{n-1}\}_S, \\ \mathbf{u}^{n+1} &= \{(\mathcal{H} - a_n)\mathbf{u}^n - b_n\mathbf{u}^{n-1}\}/b_{n+1} \end{aligned}$$

with conditions $b_0 = 0$, $b_n \geq 0$ and then the vectors $\{\mathbf{u}^m\}$ satisfy the S orthogonality

$$(\mathbf{u}^n, \mathbf{u}^m)_S = \delta_{nm}. \quad (57)$$

This process we call the generalized Lanczos (G-Lanczos) process (method). It is well known that the orthogonality relation is broken for larger n in the Lanczos method and

this is also the case here. We adopt the *modified Gram-Schmidt* reorthogonalization process in order to keep the S orthogonality. (See the results without the *modified Gram-Schmidt* reorthogonalization process in Appendix A.)

We then stop the Lanczos process up to $n = N$ and assume $\mathbf{u}^m = 0$ ($m = N + 1, N + 2, \dots$). This procedure constructs the Krylov subspace

$$K_N(\mathcal{H}, \mathbf{b}) = (\mathbf{b}, \mathcal{H}\mathbf{b}, \mathcal{H}^2\mathbf{b}, \dots, \mathcal{H}^N\mathbf{b}) \quad (58)$$

and the matrix \mathcal{H} is transformed in this subspace to a matrix of a tridiagonal form.

Starting with a natural basis $\mathbf{u}^0 = \mathbf{e}_{j_0}$, one generates vectors \mathbf{u}^n in the Krylov subspace and each vector corresponds to orthonormalized linear combination of atomic orbitals (LCAO):

$$\mathbf{u}^m \Rightarrow \varphi^m(\mathbf{r}) = \sum_j \phi_j(\mathbf{r})u_j^m. \quad (59)$$

The normalized eigenstates in the generated Krylov subspace are denoted by

$$\psi^\alpha(\mathbf{r}) = \sum_{n=0}^N \varphi^n(\mathbf{r})Q_n^{(\alpha)} = \sum_j \phi_j(\mathbf{r})w_j^\alpha, \quad (60)$$

which satisfies the Schrödinger equation

$$\sum_m \mathcal{H}_{nm}Q_m^{(\alpha)} = \varepsilon_\alpha Q_n^{(\alpha)}, \quad (61)$$

where $\mathcal{H}_{nm} = (\mathbf{u}^n, \mathcal{H}\mathbf{u}^m)_S = (\mathbf{u}^n)^\dagger H \mathbf{u}^m$.

B. Numerical test with NRL Hamiltonian for fcc Au

Chemical potential μ can be evaluated by using Eqs. (21)–(23) in the generalized Lanczos method. Calculation of the Green's function uses Eq. (13) having a double summation of atomic sites and orbitals and it consumes a long CPU time. On the contrary, the calculation of the density of states by Eq. (14) costs less CPU time. The computational efficiency will be discussed later in Sec. VI. In this section, we show several evaluated values, the density of states, the integrated density of states as functions of energies for a system of gold 864 atoms of fcc structure described by the tight-binding Hamiltonian constructed by Mehl and Papaconstantopolous.²⁴

Several evaluated values and the consistency between them are summarized in Table I. The parameters in the generalized Lanczos method are $N = 50$, the convergence criterion $\delta = 10^{-6}$ Ry in the inner CG process of $\mathbf{r}' = S^{-1}\mathbf{r}$. In GsCOCG, the imaginary small energy $\eta = 10^{-3}$ Ry, the total number of the energy integration mesh points is 3000, and the convergence criterion $\delta = 10^{-6}$ Ry in the inner CG and outer iteration procedures. The difference of the calculated total energy is of the order of 10^{-2} – 10^{-3} Ry. The scale of the band energy is 1 Ry and the relative error may be of 10^{-3} . The bold numbers in Table I are a set of consistent values in each case (for each equation determining the chemical potential) and the combination of Eqs. (17) and (19), and that of Eqs. (18) and (20) are consistent pairs of data. This consistency between the density matrix and energy density matrix is crucial for consistency between the total energy and force (see Appendix B).

TABLE I. The generalized Lanczos process applied to a system of 864 atoms of fcc Au and comparison with that of the GsCOCG. The Hamiltonian is the NRL tight-binding form (Ref. 24). The chemical potential and the total energy are in Ry units and N_{atom} is the number of atoms in the system. The bold numbers in each column are a set of consistent values.

		G-Lanczos			GsCOCG	
		μ by Eq. (21)	μ by Eq. (22)	μ by Eq. (23)	μ by Eq. (21)	
μ		0.301 086 69	0.292 665 28	0.287 009 85		0.300 608 32
	Eq. (21)	5.500 000 01	5.480 997 05	5.467 404 01	Eq. (21)	5.500 000 00
$N_{\text{tot}}/2N_{\text{atom}}$	Eq. (22)	5.518 061 52	5.499 999 98	5.486 507 39		
	Eq. (23)	5.531 622 52	5.513 521 84	5.499 999 99		
	Eq. (26)	-0.143 666 86	-0.149 267 54	-0.153 182 94	Eq. (26)	-0.143 640 84
$E_{\text{tot}}/2N_{\text{atom}}$	Eq. (27)	ρ by Eq. (17)	-0.136 471 04	-0.140 341 32	ρ by Eq. (38)	-0.125 172 55
		ρ by Eq. (18)	-0.136 941 55	-0.140 820 23		
	Eq. (28)	π by Eq. (19)	-0.136 470 94	-0.140 341 23	π by Eq. (39)	-0.143 640 84
		π by Eq. (20)	-0.136 941 46	-0.140 820 14		

In the GsCOCG method, calculation of Eqs. (38) and (39) needs ε integration of $\rho_{ij}(\varepsilon)$ and the numerical integration causes a certain error in the integration of the tail of the spectra. Once we reduce the value of η and increase the ε points of the integration, this discrepancy can be reduced. In the generalized Lanczos method, the combination of Eqs. (23), (18), and (20) is the best scheme, since we do not use the numerical energy integral.

Figure 4 shows the partial density of states and integrated density of states for s , p , and d orbitals. Those by the generalized Lanczos method are compared with exact results. The peak positions and the tails overlap excellently and we can conclude that the generalized Lanczos method can be a powerful and convenient tool. One must note that the exact results are more smooth in the central energy region since the correct density of states is more dense in this energy region. In other words, the exact results reserve the entire profile with 864×9 peaks but, on the contrary, those by the generalized Lanczos method reserve the profiles with $51 (= N + 1)$ peaks or the density of states is expressed as a polynomial function of energy of the order 51 in the present calculation.

V. GENERALIZED ARNOLDI PROCESS AND DENSITY OF STATES

A. Generalized Arnoldi process

We can construct the Krylov subspace, starting with a natural basis $\mathbf{u}^0 = \mathbf{e}_{j_0}$, by using the Hamiltonian matrix H as^{19,27}

$$\mathbf{l}^{n+1} = H\mathbf{u}^n, \quad (62)$$

$$\mathbf{k}^{n+1} = \mathbf{l}^{n+1} - \sum_{m=0}^n \mathbf{u}^m (\mathbf{u}^m, \mathbf{l}^{n+1})_S, \quad (63)$$

$$\mathbf{u}^{n+1} = \frac{\mathbf{k}^{n+1}}{(\mathbf{k}^{n+1}, \mathbf{k}^{n+1})_S^{1/2}}. \quad (64)$$

This is the Arnoldi process and we call it the generalized Arnoldi (G-Arnoldi) method. The generalized Arnoldi method

generates the Krylov subspace

$$\begin{aligned} K_{N+1}(H; \mathbf{b}) &= \text{Span}\{\mathbf{b}, H\mathbf{b}, H^2\mathbf{b}, \dots, H^N\mathbf{b}\} \\ &= \text{Span}\{\mathbf{u}^0, \mathbf{u}^1, \mathbf{u}^2, \dots, \mathbf{u}^N\}. \end{aligned} \quad (65)$$

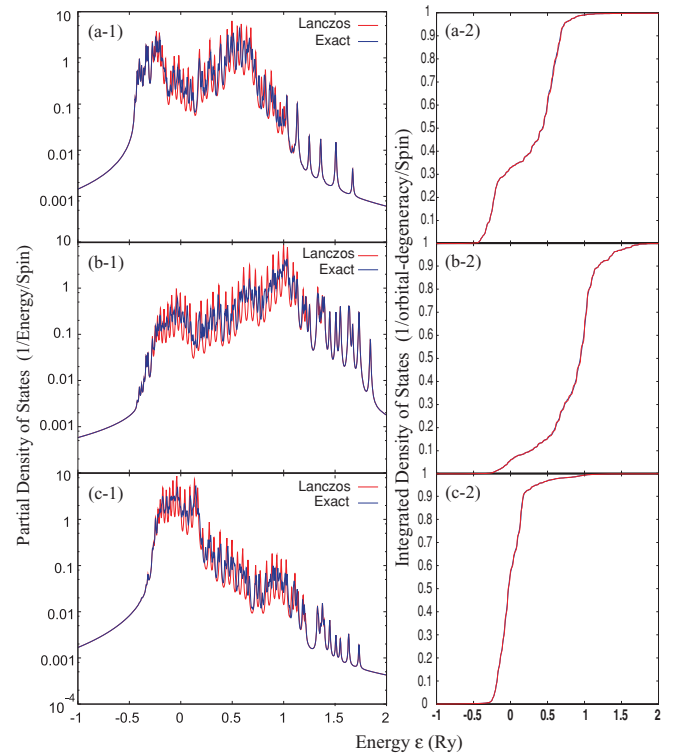


FIG. 4. (Color online) Partial density of states (pDOS), normalized to unity, and integrated density of states (IDOS) for a system of Au 864 atoms by the NRL tight-binding Hamiltonian (Ref. 24). Comparison is between those of the generalized Lanczos method (red solid lines) and those of the exact ones (blue solid lines). (a-1) and (a-2): pDOS and IDOS for s orbitals. (b-1) and (b-2): pDOS and IDOS for p orbitals. (c-1) and (c-2): pDOS and IDOS for d orbitals. $\eta = 5.0 \times 10^{-3}$ Ry.

TABLE II. The generalized Arnoldi process applied to a system of 864 atoms of fcc Au and comparison with that of the GsCOCG. The Hamiltonian is the NRL tight-binding form (Ref. 24). The chemical potential and the total energy are in Ry units and the N_{atom} is the number of atoms in the system. The bold numbers in each column are a set of consistent values.

		G-Arnoldi			GsCOCG	
		μ by Eq. (21)	μ by Eq. (22)	μ by Eq. (23)	μ by Eq. (21)	
μ		0.303 906 79	0.292 871 98	0.286 461 36		0.300 608 32
	Eq. (21)	5.500 000 02	5.479 717 90	5.465 817 73	Eq. (21)	5.500 000 00
$N_{\text{tot}}/2N_{\text{atom}}$	Eq. (22)	5.517 608 87	5.500 000 01	5.486 509 81		
	Eq. (23)	5.531 166 53	5.513 519 49	5.499 999 99		
	Eq. (26)	-0.142 300 73	-0.148 265 63	-0.152 231 79	Eq. (26)	-0.143 640 84
$E_{\text{tot}}/2N_{\text{atom}}$	Eq. (27)	ρ by Eq. (17)	-0.135 144 34	-0.138 954 98	ρ by Eq. (38)	-0.125 172 55
		ρ by Eq. (18)	-0.135 611 05	-0.139 429 96		
	Eq. (28)	π by Eq. (19)	-0.135 144 34	-0.138 954 98	π by Eq. (39)	-0.143 640 84
		π by Eq. (20)	-0.135 611 05	-0.139 429 96		

The generated vector \mathbf{u}^m corresponds to orthonormalized LCAO

$$\varphi^m(\mathbf{r}) = \sum_j \phi_j(\mathbf{r}) u_j^m \quad (66)$$

as in the G-Lanczos method. An eigenfunction $\psi^\alpha(\mathbf{r}) = \sum_n \varphi^n(\mathbf{r}) Q_n^{(\alpha)}$ satisfies the Schrödinger equation

$$\sum_m \tilde{H}_{nm} Q_m^{(\alpha)} = \varepsilon_\alpha Q_n^{(\alpha)}, \quad (67)$$

where $\tilde{H}_{mn} = \langle \varphi^m | \hat{H} | \varphi^n \rangle = (\mathbf{u}^m)^\dagger H \mathbf{u}^n$ and \tilde{H} is an upper Hessenberg matrix. We can say that this procedure is a kind of generalization of the subspace diagonalization of the Krylov subspace developed before.¹³

B. Numerical test with NRL Hamiltonian for fcc Au

We summarize, in Table II, several evaluated values and consistency between them, in comparison with the results of the GsCOCG. The system is of 864 atoms of fcc Au by the NRL tight-binding Hamiltonian.²⁴ The bold numbers in the table are a set of consistent results in each calculation of the chemical potential. $N = 50$ for the generalized Arnoldi process. Data of GsCOCG are the same as in Table I. The calculated values of the total energies agree with those by the generalized Lanczos method, and the overall difference is less than 1% as shown in Table I.

Figure 5 shows the partial density of states and the integrated density of states as functions of energies. The peak positions are deviated slightly from those by the exact calculation, which one could make smaller by increasing a dimension N of the Krylov subspace.

VI. COMPARISON AMONG GSCOCG AND G-LANCZOS AND G-ARNOLDI METHODS

A. Convergence

The dimension of the Krylov subspace in GsCOCG, G-Lanczos, or G-Arnoldi methods equals to $N + 1$, where N is the maximum iteration step. The GsCOCG method is a very accurate method if one achieves the iteration to have enough small residual norm (e.g., $\delta = 10^{-6}$ Ry). In Fig. 2, we have

shown the convergence behavior of the residual norms with different seed energies and until it reaches a much smaller convergence region. One should use the same iteration criteria both in the inner CG and outer procedures in the GsCOCG method. It sometimes happens that the resultant DOS shows an unphysical behavior, e.g., negative values of DOS, if one stops the iteration steps before enough convergence in the GsCOCG method. On the other hand, the G-Lanczos and G-Arnoldi methods never give such unphysical DOS, even

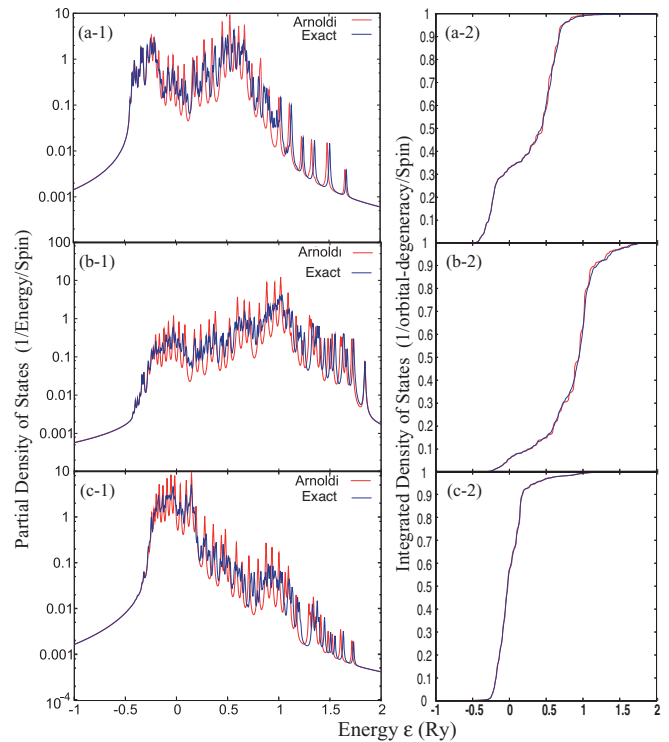


FIG. 5. (Color online) Partial density of states, normalized to unity, and integrated density of states. Comparison is between those of the generalized Arnoldi method (red solid lines) and those of the exact ones (blue solid lines) for a system of Au 864 atoms by the NRL tight-binding Hamiltonian (Ref. 24). (a-1) and (a-2): pDOS and IDOS for s orbitals. (b-1) and (b-2): pDOS and IDOS for p orbitals. (c-1) and (c-2): pDOS and IDOS for d orbitals. $\eta = 5.0 \times 10^{-3}$ Ry.

TABLE III. Chemical potential and the total energy (in Ry units) of systems of 864 and 256 atoms of fcc Au (Ref. 24) by three different methods. The values of ρ in the G-Lanczos and G-Arnoldi methods are evaluated by Eq. (18).

		G-Lanczos	(864 atoms)	(256 atoms)
μ	Eq. (22)		0.292 665 28	0.287 541 33
$E_{\text{tot}}/2N_{\text{atom}}$	Eq. (27)		-0.136 471 04	-0.135 876 39
		G-Arnoldi	(864 atoms)	(256 atoms)
μ	Eq. (22)		0.292 871 98	0.288 621 49
$E_{\text{tot}}/2N_{\text{atom}}$	Eq. (27)		-0.135 144 34	-0.134 661 95
		GsCOCG	(864 atoms)	(256 atoms)
μ	Eq. (21)		0.300 608 32	0.294 715 35
$E_{\text{tot}}/2N_{\text{atom}}$	Eq. (26)		-0.143 640 84	-0.143 319 25

if one stops at a small iteration step because of the expression of Eq. (13). Furthermore, the first N moments are preserved correctly in the energy spectra of the G-Lanczos method. In the spectrum of this model by the exact calculation, we observe about 40 prominent peaks and then we use $N = 50$ in the calculations of the G-Lanczos and G-Arnoldi procedures. This is presumably the reason why the peak positions and detailed profiles in the spectra of the G-Lanczos method show excellent agreement with those of the exact calculation. The G-Lanczos method needs the Gram-Schmidt reorthogonalization, and also it is necessary to have enough convergence in the inner CG procedure. The G-Arnoldi method does not need such a reorthogonalization procedure since one solves the eigenvalue problem in that subspace.

In condensed matters, the width of the valence and/or conduction bands W may be of the order of 1 Ry. Then, when the number of atoms is N_{atom} , we can estimate the separation of each energy level as of the order of $W/(9 \times N_{\text{atom}})$. Presumably, 10% of this separation would be enough accuracy in the energy scale. In our case, with $N_{\text{atom}} \approx 1000$, the convergence criterion can be chosen as $0.1 \times W/(9 \times N_{\text{atom}}) \approx 0.1 \times 1/9000 \approx 10^{-5}$ Ry. We also observed that the maximum iteration steps are almost the same for the convergence criterion $\delta = 10^{-5}$ and $\delta = 10^{-6}$ in the GsCOCG and G-Lanczos methods. This is the reason why we choose $\delta = 10^{-6}$ Ry.

We compare the results of the chemical potential and the total band energy of systems of 256 and 864 atoms in Table III. The difference of the chemical potential μ is of the order of 10^{-3} Ry and that of the total band energy E_{tot} is of the order of 10^{-4} Ry. The level separation in the 256-atom system can be estimated as $1.0/(9 \times 256) \approx 4 \times 10^{-4}$ Ry and that in 864-atom system as 10^{-4} Ry. The difference in the chemical potential of two systems of different sizes is due to the difference of the total number of levels, which change the value of the chemical potential sensitively. On the other hand, the difference of E_{tot} is just the quantity related to the overall spectrum, and we can see an excellent convergence of the results of $N = 50$.

Figure 6 shows the actual convergence behavior of IDOS by the G-Lanczos and G-Arnoldi methods. The agreement

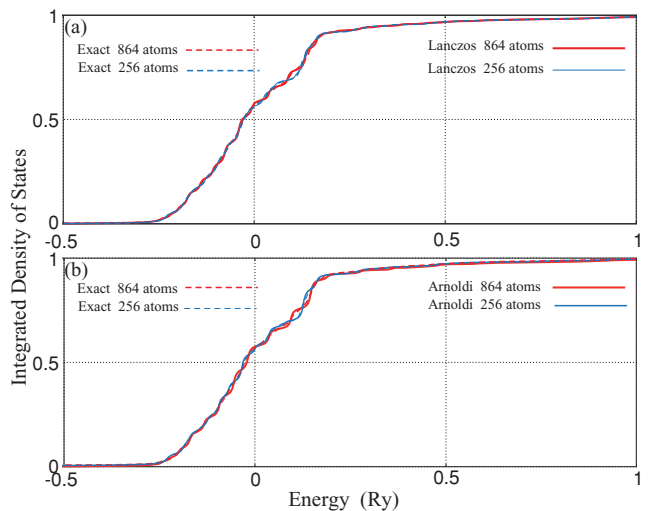


FIG. 6. (Color online) Comparison of IDOS of d orbitals for systems of Au 256 and 864 atoms by the NRL tight-binding Hamiltonian (Ref. 24). (a) The G-Lanczos (solid line) and exact calculation (chain line) for 864 atoms (red) and 256 (blue) atoms. (b) The G-Arnoldi (solid line) and exact calculation (chain line) for 864 atoms (red) and 256 (blue) atoms. The agreement between the results by the G-Lanczos or G-Arnoldi methods and those by the exact calculation is excellent.

between the results by the G-Lanczos or G-Arnoldi methods and those by the exact calculation is excellent both for systems of 864 atoms and those of 256 if we adopt $N = 50$. The most apparent difference appears in the IDOS curves of the exact calculation of systems of 256 and 865 atoms in the mid-energy region, and the calculated results by our methods present this difference with complete fidelity.

B. CPU times

We summarize, in Table IV, the CPU times (by using single CPU of the standard workstation) for (s orbitals) D_{ii} of the generalized Lanczos and the generalized Arnoldi methods with Eq. (14), that of GsCOCG with Eq. (37), and that of the exact diagonalization method for the NRL Hamiltonian of fcc Au system of 256 and 864 atoms.²⁴ The total number of orbitals equals nine times the total number of atoms (1 s , 3 p 's, and 5 d 's). We use, in the inner CG process of the generalized Lanczos method, the convergence criterion $\delta = 10^{-6}$ Ry. Two numbers in the row of the CPU time are referred to those of $N = 50$ and 100, respectively, for the G-Lanczos and G-Arnoldi methods, although the results of $N = 100$ almost coincide with those of $N = 50$. For GsCOCG (with shifted 3000 energy points), the data shown here are those of $\delta = 10^{-6}$ Ry both for in the inner and outer iteration processes. The repeated time of the inner CG process ($S^{-1}\mathbf{x}$ part) in the GsCOCG and G-Lanczos method is 10–11. (Repeated time of 25–27 is needed for $\delta = 10^{-18}$ Ry.)

The system size dependence of the CPU time is linear for the generalized Arnoldi and Lanczos methods, bilinear for the method, and cubic for the exact calculation. The generalized Arnoldi method is extremely efficient in electronic structure calculations of extra-large systems with several hundred thousand atoms.

TABLE IV. CPU times by using a standard single CPU workstation for a system of gold 256 atoms (Au256) and gold 864 atoms (Au864) by the NRL tight-binding Hamiltonian (Ref. 24).

Au 256		CPU times (s)	
G-Arnoldi	Main part	0.52	1.11
	Total	1.59	3.20
G-Lanczos	Inner CG	2.04	3.89
	Main part	2.89	5.60
	Total	3.92	7.62
GsCOCG	Seed		13.67
	Shifted		7.53
	Total		21.20
Exact			57.60
Au 864		CPU times (s)	
G-Arnoldi	Main part	1.94	3.76
	Total	3.00	6.00
G-Lanczos	Inner CG	7.93	15.13
	Main part	10.87	21.13
	Total	11.93	23.31
GsCOCG	Seed		140.89
	Shifted		108.36
	Total		249.15
Exact			2111.51

C. Applicability to large-scale electronic structure calculations and MD simulations

In the exact calculation and GsCOCG methods, calculations of physical properties, such as the density matrix, the energy density matrix, and chemical potential, require the numerical integration as in Eqs. (21), (26), (38), and (39). Therefore, to keep high accuracy, the integration needs fine energy mesh points. On the other hand, the generalized Lanczos or Arnoldi methods use the simple summation of the eigenstates in the mapped subspace in Eqs. (22), (23), and (17)–(20). These two methods do not consume the CPU time and give stable values of the density matrix and the energy density matrix.

The CPU times per one MD step are, for these models, a few seconds by the generalized Lanczos and Arnoldi methods. From the above comparison among various viewpoints, we can conclude that the generalized Lanczos method or the generalized Arnoldi method are very suitable to large-scale electronic structure calculations and MD simulation of several tens of thousands atoms and a long MD step. On the other hand, the GsCOCG method can give excellently rigorous results with more CPU times and may be applicable to problems of a fixed atomic configuration (but not for the MD simulation).

The GsCOCG method is based on the three-term recursive equations and we need to store three generated vectors at each recursive process. Of course, when the sizes of the Hamiltonian and overlap matrices are extremely large and the memory size becomes a serious obstacle (although much smaller consumption than the exact diagonalization method), we should invent other methods of much faster convergence and smaller cost of memory size.

The convergence criterion $\delta = 10^{-5}$ might correspond to the range of neighboring 1000 atoms, as already discussed, and we do not observe any clear difference between results by

our methods and the exact calculations. Even when we should discuss some physics of nanoscale systems, the electronic structure is determined by some nearby surroundings. This idea we call *near-sitedness*.²⁸ Even when we have to deal with much larger systems, we can use a smaller interaction range than the system size due to the near-sitedness. Presumably, more serious problems of the system size occur in some specific problems, for example, *entire* calculation of nanodevice or the electron-strain field interactions such as fracture propagation^{1,2} and dislocation.²⁹

VII. CONCLUSION

We have derived several efficient and accurate algebraic methods to calculate the Green's functions, total and partial density of states, and total band energy in case of nonorthogonal atomic orbitals. The method is very general.

We have investigated the accuracy and efficiency by showing numerical data with different numerical procedures. The GsCOCG is very accurate with less consumption than the exact diagonalization, but may not be appropriate for long MD-step simulations. The generalized Lanczos method becomes applicable to actual large systems with the modified Gram-Schmidt reorthogonalization to maintain the orthogonality

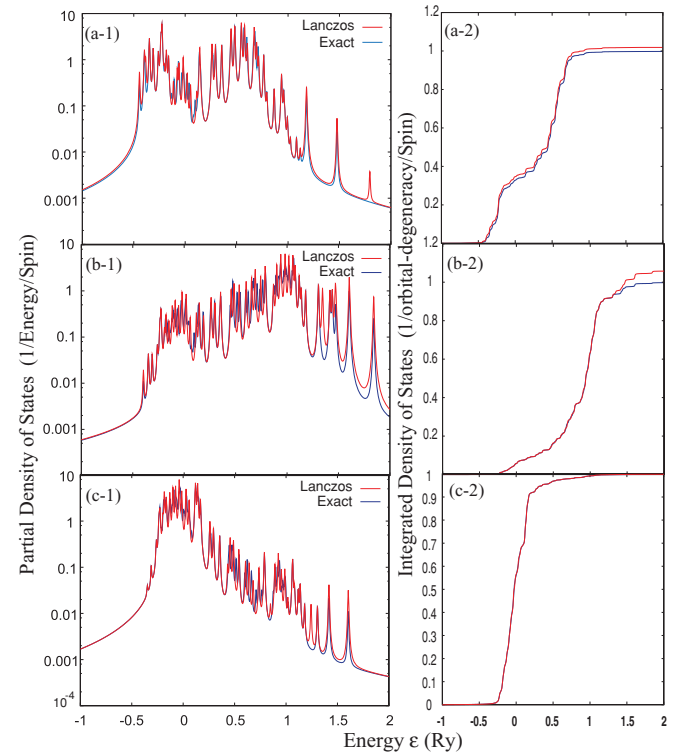


FIG. 7. (Color online) Partial density of states and integrated ones without the modified Gram-Schmidt reorthogonalization of the generalized Lanczos method (red solid lines) and those by the exact ones (blue solid lines) for a system of Au 256 atoms by the NRL tight-binding Hamiltonian (Ref. 24). $N = 50$. (a-1) and (a-2): pDOS and IDOS for s orbitals. (b-1) and (b-2): pDOS and IDOS for p orbitals. (c-1) and (c-2): pDOS and IDOS for d orbitals. One should note that the normalization of the integrated density of states is broken without reorthogonalization procedure and that some “ghost” peaks appear due to incorrect mixing of states. $\eta = 5.0 \times 10^{-3}$ Ry.

of generated basis vectors. Then, the generalized Arnoldi and Lanczos methods are accurate and efficient, and their CPU times depend linearly upon the system size. Therefore, these two methods would be the most suitable to the large-scale electronic structure calculations and MD simulations. A crucial point we should point out finally is the fact that the G-Lanczos and G-Arnoldi methods do not adopt any numerical integration in energy, which leads to additional numerical error.

ACKNOWLEDGMENTS

T. Fujiwara expresses sincere thanks to TOYOTA Motor Corporation for the financial support. Numerical calculation was partly carried out using the supercomputer facilities of the Institute for Solid State Physics, University of Tokyo.

APPENDIX A: REORTHOGONALIZATION BY MODIFIED GRAM-SCHMIDT METHOD

The three-term recursive relation in the generalized Lanczos method guarantees theoretically the automatic S orthogonalization. However, the orthogonality is broken in the numerical calculation procedure. This problem causes several issues such as the existence of constant background of error in the spectrum,¹⁴ appearance of “ghost” structure in spectrum due to erroneous mixing of states, and a broken normalization of the partial density of states.

Figure 7 shows the examples of this broken orthonormality in a system of 256 atoms of fcc Au by using the NRL Hamiltonian. One can see the “ghost” peaks [e.g., at $\varepsilon \simeq 1.8$ Ry in (a-1), at $\varepsilon \simeq 1.25 - 1.3$ Ry in (b-1) and (c-1)], and broken normalization [e.g., in (a-2) and (b-2)]. These problems are solved by the reorthogonalization with the modified Gram-Schmidt method.

APPENDIX B: CONSISTENCY BETWEEN THE TOTAL ENERGY MINIMUM AND A VANISHING FORCE

We should construct our eigenstates in a small subspace, and a certain numerical error is unavoidable in evaluated total energy and force. Even in this case, the consistency between the total band energy minimization and a vanishing atomic force is the most important in the electronic structure calculation in equilibrium atom configuration. In the framework of the tight-binding model, the force (due to band energy) acting on an atom I is evaluated by a formula

$$F_I = -2 \sum_{ij} \left(\rho_{ij} \frac{\partial H_{ij}}{\partial \mathbf{R}_I} - \pi_{ij} \frac{\partial S_{ij}}{\partial \mathbf{R}_I} \right), \quad (\text{B1})$$

which can be rewritten, with only an assumption of the eigenstate property Eq. (8) in the mapped subspace, as

$$F_I = -2 \frac{\partial}{\partial \mathbf{R}_I} \left\{ \sum_{ij} (\rho_{ij} H_{ij}) - \sum_{ij} (\pi_{ij} S_{ij}) \right\} - \frac{\partial}{\partial \mathbf{R}_I} \sum_{\alpha} f(\varepsilon_{\alpha}) \varepsilon_{\alpha}. \quad (\text{B2})$$

Therefore, calculated atomic and electronic configuration of the minimum total energy is consistent with that of vanishing atomic force if the identity $\sum_{ij} (\rho_{ij} H_{ij}) = \sum_{ij} (\pi_{ij} S_{ij})$ is satisfied always in any atomic configuration. It should be noted that the above equality is satisfied in the mapped subspace as described in II C 2. It is important in the actual calculating procedure that we should use the consistent pair of equations as (17) and (19) or (18) and (20).

*Present address: Institute of Mechanics, Chinese Academy of Sciences, Beijing, China.

†fujiwara@coral.t.u-tokyo.ac.jp

¹T. Hoshi and T. Fujiwara, *J. Phys. Soc. Jpn.* **72**, 2429 (2003).

²T. Hoshi, Y. Iguchi, and T. Fujiwara, *Phys. Rev. B* **72**, 075323 (2005).

³Y. Iguchi, T. Hoshi, and T. Fujiwara, *Phys. Rev. Lett.* **99**, 125507 (2007).

⁴T. Hoshi and T. Fujiwara, *J. Phys. Condens. Matter* **21**, 272201 (2009).

⁵S. Goedecker, *Rev. Mod. Phys.* **71**, 1085 (1999).

⁶S. Goedecker and L. Colombo, *Phys. Rev. Lett.* **73**, 122 (1994).

⁷W. Yang, *Phys. Rev. Lett.* **66**, 1438 (1991); T. Ozaki, *Phys. Rev. B* **74**, 245101 (2006).

⁸X.-P. Li, R. W. Nunes, and D. Vanderbilt, *Phys. Rev. B* **47**, 10891 (1993).

⁹F. Mauri, G. Galli, and R. Car, *Phys. Rev. B* **47**, 9973 (1993).

¹⁰C.-K. Skylaris, P. D. Haynes, A. A. Mostofi, and M. C. Payne, *J. Chem. Phys.* **122**, 084119 (2005).

¹¹J. M. Soler, E. Artacho, J. D. Gale, A. García, J. Junquera, P. Ordejón, and D. Sánchez-Portal, *J. Phys. Condens. Matter* **14**, 2745 (2002).

¹²P. Ordejón, *Comput. Mater. Sci.* **12**, 157 (1998).

¹³R. Takayama, T. Hoshi, and T. Fujiwara, *J. Phys. Soc. Jpn.* **73**, 1519 (2004).

¹⁴R. Takayama, T. Hoshi, T. Sogabe, S.-L. Zhang, and T. Fujiwara, *Phys. Rev. B* **73**, 165108 (2006).

¹⁵T. Sogabe, T. Hoshi, S.-L. Zhang, and T. Fujiwara, *Electronic Trans. Numer. Anal. (ETNA)* **31**, 126 (2008).

¹⁶T. Sogabe, T. Hoshi, S.-L. Zhang, and T. Fujiwara, in *Frontiers of Computational Science*, edited by Y. Kaneda, H. Kawamura, and M. Sasai (Springer Verlag, Berlin, 2007), pp. 189–195.

¹⁷C. Lanczos, *J. Res. Nat. Bur. Stand. (US)* **45**, 255 (1950); **49**, 33 (1952).

¹⁸R. Haydock, in *Solid State Physics*, edited by H. Ehrenreich, F. Seitz, and D. Turnbull (Academic, New York, 1980), Vol. 35, pp. 225–228.

¹⁹*Templates for the Solution of Algebraic Eigenvalue Problems*, edited by Z. Bai, J. Demmel, J. Dongarra, A. Ruhe, and H. van der Vorst (SIAM, Philadelphia, 2000), Chap. 5.

²⁰M. Elstner, D. Porezag, G. Jungnickel, J. Elsner, M. Haugk, Th. Frauenheim, S. Suhai, and G. Seifert, *Phys. Rev. B* **58**, 7260 (1998).

²¹T. Fujiwara, T. Hoshi, and S. Yamamoto, *J. Phys. Condens. Matter* **20**, 294202 (2008).

- ²²T. Sogabe and S.-L. Zhang, International Conference on Numerical Analysis and Scientific Computing with Applications, Agadir, Morocco, 2009 (unpublished); T. Sogabe, T. Hoshi, S.-L. Zhang, and T. Fujiwara (unpublished).
- ²³A. Frommer, *Computing* **70**, 87 (2003).
- ²⁴M. J. Mehl and D. A. Papaconstantopoulos, *Phys. Rev. B* **54**, 4519 (1996); F. Kirchoff, M. J. Mehl, N. I. Papanicolaou, D. A. Papaconstantopoulos, and F. S. Khan, *ibid.* **63**, 195101 (2001).
- ²⁵S. Yamamoto, T. Sogabe, T. Hoshi, S.-L. Zhang, and T. Fujiwara, *J. Phys. Soc. Jpn.* **77**, 114713 (2008).
- ²⁶T. Ozaki and K. Terakura, *Phys. Rev. B* **64**, 195126 (2001).
- ²⁷T. Hoshi, S. Nishino, S. Yamamoto, T. Fujiwara, Y. Zempo, M. Ishida, T. Sogabe, and S.-L. Zhang (unpublished).
- ²⁸W. Kohn, *Phys. Rev. Lett.* **76**, 3168 (1996).
- ²⁹M. Miyata and T. Fujiwara, *Phys. Rev. B* **63**, 045206 (2001).